EXPERIMENTS ON INTERNAL WAVE RESONANCE IN PERIODICALLY FORCED LAKES

LEON BOEGMAN

Department of Civil Engineering, Queen's University
Kingston, ON, Canada, K7L 3N6

GREGORY N. IVEY

School of Environmental Systems Engineering, University of Western Australia
Crawley, WA, Australia, 6009

Abstract. Laboratory experiments were conducted to determine the steady state internal wave response of a periodically forced long and narrow lake. The system is two-layer stratified and is subjected to periodic forcing over a wide frequency range. The ratio of the forcing frequency (f) to horizontal mode-one (H1) internal seiche frequency (f_{H1}) governs the system response. For $f \geq 2f_{H1}$, higher-mode internal seiches were observed; for $f \leq (2/3)f_{H1}$, a non-resonant forced H1 internal seiche was observed; and for $(2/3)f_{H1} < f < 2f_{H1}$, a resonant H1 internal seiche was observed. For the resonant regime, progressive nonlinear internal waves (e.g. solitary waves) formed upon the H1 seiche when the inverse Wedderburn number, $W^{-1} > 0.03$ (W^{-1} is the ratio of the wind-induced thermocline set-up to the thermocline depth). The nonlinear internal waves will break upon sloping topography at the lake perimeter, thus energizing the benthic boundary layer. Conversely, for $W^{-1} > 0.5$, Kelvin-Helmholtz instabilities were observed to form within the progressive nonlinear internal waves, leading to diapycnal mixing (10^{-2} m^{2}s$^{-1} < K_\rho < 10^{-4}$ m^{2}s^{-1}) within the basin interior.

1. Introduction

The periodicity in weather patterns creates over-lake wind fields that occur at regular frequencies. For example, the winds over Lake Erie have periodicities of 10 d and 24 h, associated with frontal weather systems and diurnal heating/cooling, respectively. When the forcing frequency matches that of one of the natural frequencies of the basin-scale internal seiche modes, resonant amplification will result. Seasonal heating and deepening of the thermocline adjust the natural frequencies relative to the forcing frequencies, thus tuning the system into and out of resonance even when the forcing frequency is unchanged [1]. Field observations (e.g. [10]) show that resonance is particularly effective in amplifying the response of the second vertical mode and even horizontal modes not naturally energized by a basin-scale wind-induced thermocline setup [4].

Resonance also appears to increase steepening of the basin-scale internal seiche modes, thus enhancing energy flux to progressive nonlinear internal waves (NLIWs) [13]; both at the basin-scale (e.g. surges and bores) and at small-scale and high-frequency (e.g. solitary waves)[6, 4]. Energy flux to high-frequency NLIWs leads to diapycnal mixing within the basin interior [5] and where high-frequency NLIWs shoal on sloping topography at the lake perimeter [9, 3].

The objectives of the present study are two-fold. Using a laboratory experiment, we aim to describe the internal wave response of a periodically forced two-layer basin and to quantify the energy flux pathways from the applied forcing condition through the internal wave field to ultimate dissipation and mixing at turbulent scales. These results will then be generalized to the field scale.

2. Theory and nomenclature

During the summer months, a stratified lake will typically possess a layered structure consisting of an epilimnion, a metalimnion and a hypolimnion. If the thickness of the metalimnion is small compared to the other layers, then the lake may be approximated as a simple two-layer system of depth h_1 and density ρ_1 over depth h_2 and density ρ_2, where $H = h_1 + h_2$ is the total depth, B the basin width and L the basin length. The internal response of the lake to a wind stress can be quantified by the inverse Wedderburn number, $W^{-1} \sim \eta_o/h_1$ [6], where η_o is the initial amplitude of the wind-induced thermocline disturbance. Upon relaxation of the wind stress, the period of the resulting horizontal mode one (H1) internal

standing seiche is $T_i = 2L/c_o$, where $c_o = \sqrt{g' h_1 h_2 / H}$ is the linear long-wave speed and $g' = g(\rho_2 - \rho_1)/\rho_2$ the reduced gravity at the interface.

3. Experimental methods

The laboratory experiments were conducted in a sealed rectangular acrylic tank ($L = 600$ cm, $H = 29$ cm and $B = 30$ cm) filled with a two-layer stratification of fresh and saline water [6]. A typical geophysical stratification was introduced with a thinner upper-layer ($h_1/H = 0.3$) allowing for the formation of high-frequency NLIWs of depression. The system was periodically forced along the longitudinal axis about a central pivot point using an eccentric crank and arm attached to an electric motor (figure 1a). Over each forcing period, the motion of the crank arm smoothly rotated the end of the tank through a prescribed vertical displacement (Δ_T) before being returned to the horizontal position. Through this procedure, the set-up and subsequent relaxation resulting from periodic wind-stress events acting in a consistent direction along the longitudinal axis was simulated. In each experiment the system was forced until steady state was achieved. For experiments where significant mixing of the interface was observed, the experiments were terminated prior to appreciable thickening of the interface.

To visualize the flow field, digital images of the tank were acquired using a Canon MV-X2i digital video camera. For these experiments, the lower layer was seeded with red dye and the tank was illuminated with backlight from halogen lamps (figure 1b). The vertical displacements of the density interface were measured two ultrasonic wavegauges (LEGI) distributed longitudinally along the tank at locations WGA and WGB. The wavegauges logged data to a personal computer at 10 Hz through a 16-bit analog-to-digital converter (National Instruments PCI-MIO-16XE-50). A typical timeseries of interfacial displacement is shown in figure 1c. The density structure was measured by vertically traversing two FP07 Fast Conductivity and Temperature Sensors (Precision Measurement Engineering) through the fluid. The direct and gradient resistances were converted to output voltages in a conditioning box, then digitized at 100 Hz using a using the 16-bit analog-to-digital converter and logged to a personal computer. The voltages were converted to density by calibration against an Anton-Paar densimeter (DMA60). Measurements were made with the fluid quiescent both before and after the forcing event and this enabled the computation of the increase in potential energy of the system as a result of any turbulent mixing [9].

4. Results

4.1. *Flow field*

At the beginning of each experiment the flow was driven by the baroclinic pressure gradient generated by the rocking of the tank. With time, the flow evolved into a spectrum of internal waves, composed of basin-scale internal seiches, a progressive internal surge and high-frequency NLIWs, consistent with field and laboratory results [6, 3]. The ratio of (f) to f_{H1} governed the system response and three regimes were identified (figure 2). For $f \geq\sim 2f_{H1}$, higher-mode internal seiches were predominantly observed; for $f \leq\sim (2/3)f_{H1}$, a non-resonant forced H1 internal seiche was predominantly observed; and for $\sim (2/3)f_{H1} < f <\sim 2f_{H1}$, a resonant H1 internal seiche anf NLIWs were observed. Under resonant conditions, progressive high-frequency NLIWs (e.g. solitary waves) formed upon the resonating H1 seiche and Kelvin-Helmholtz instabilities were observed to form within the progressive nonlinear internal waves, leading to diapycnal mixing within the basin interior. The complex combination of these modes is shown spatially in the video data (figure 1b) and temporally at discrete locations in the wavegauge data (figure 1c).

4.2. *Internal wave energetics*

For selected resonantly forced experiments (table 1), the internal wave field was decomposed into an H1 seiche, a surge and NLIW components following the methods of [4, 3]. Briefly, this was accomplished by separating the three component wave

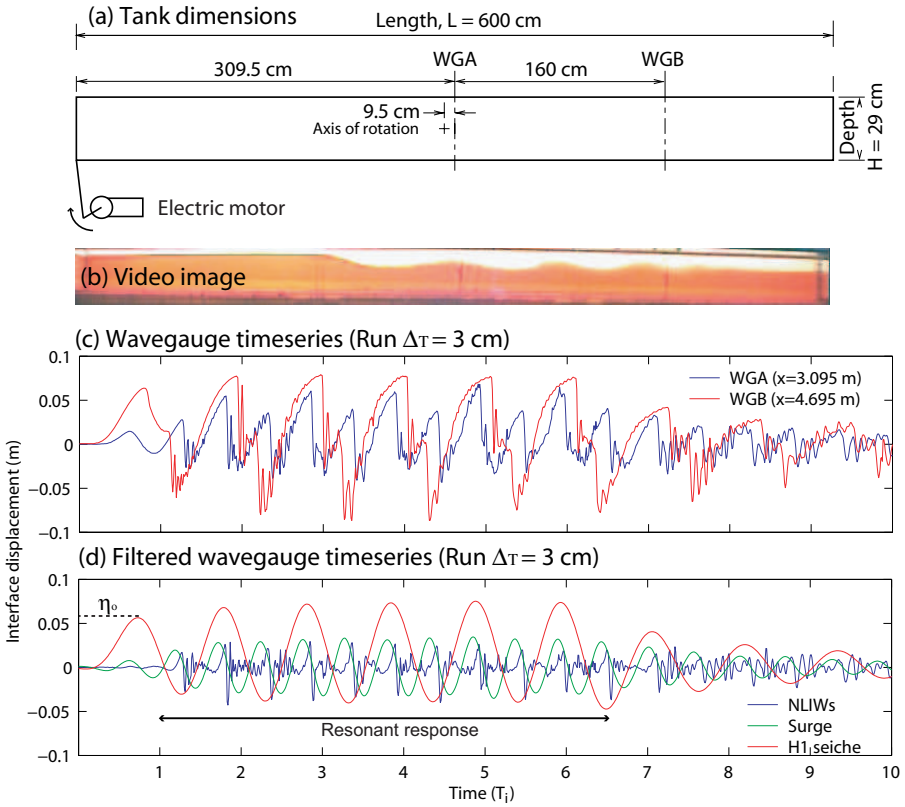

Figure 1. (a) Schematic diagram of the experimental set-up. The ultrasonic wavegauges were located at the positions marked WGA and WGB. (b) Video image showing the standing seiche, progressive surge and NLIWs. (c) Time series of the observed interface displacement. (d) Filtered time series of the interface displacement showing the component H1 seiche, nonlinear surge and NLIWs. During resonance the H1 seiche is vertically displaced from the equilibrium position due to the steady baroclinic tilt.

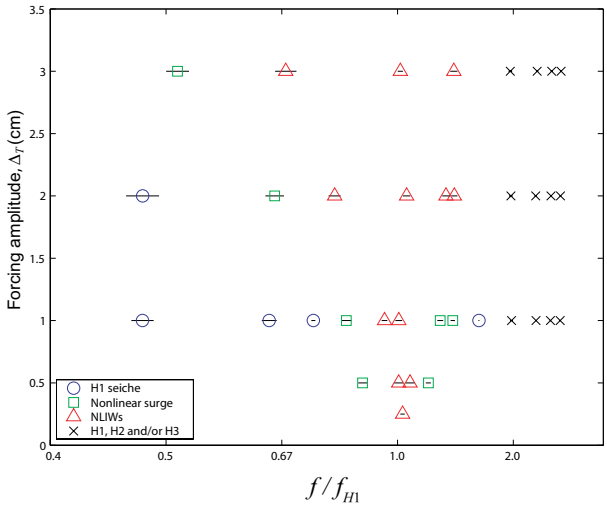

Figure 2. Regime diagram showing the dominant internal wave response under periodic forcing conditions. Note that for Δ_T = 1, 2 and 3 cm, η_o = 2.2, 4.8 and 7.3 cm and W^{-1} = 0.25, 0.55 and 0.84, respectively (table 1). Error bars denote the variation in forcing during an experiment (mean ± standard deviation).

modes through selective filtering of the timeseries, which are discrete in frequency space. The energy in the surge and NLIWs was then quantified by integrating the filtered timeseries over the characteristic timescale during which one wave length or packet length, respectively, progressed through a wavegauge [9]. The H1 seiche is not progressive and so its maximum amplitude, occurring at the end walls, was determined (as was η_o) by projecting a cosine function fitted in a least-squares sense to the filtered data at WGA and WGB. The seiche energy was attained by decomposing the resulting timeseries at the end-wall into the component waves forming the standing wave pattern, integrating as above and summing the energy in the two components.

Table 1
Summary of experimental runs: $h_1 \approx 8.7$ cm, $h_2 \approx 20.3$ cm, $\rho_1 \approx 1000$ kgm^{-3} and $\rho_2 \approx 1020$ kgm^{-3}. The density difference between the upper and lower layers $\rho_2 - \rho_1 \approx 20$ kg m^{-3} ($\pm$ 2 kgm^{-3}), $c_o \approx 0.11$ ms^{-1}, $g' \approx 0.20$ Nkg^{-1} and $T_i \approx 110$ s. In each run the tank was forced for 6 cycles. The value in parenthesis is considered inaccurate, as during resonance the wavegauge signal was contaminated with Kelvin-Helmholtz instabilities (figure 3) leading to poor measurement of the NLIW signal (figure 1d $t < 6T_i$ relative to $t > 6T_i$). K_ρ and ϵ are averages over δ_ρ and T_i. The energy in the baroclinic tilt, H1 seiche, surge and high-frequency NLIWs are denoted by E_T, E_{H1}, E_S and E_{HF}, respectively.

Δ_T	W^{-1}	P	E_T/P	E_{H1}/P	E_S/P	E_{HF}/P	R_f	ϵ	K_ρ
cm		Jm^{-1}cycle^{-1}	%	%	%	%		Wkg^{-1}	m^{2}s^{-1}
1	0.25	0.10	8	337	110	151	0.03	0.06	2.0×10^{-4}
2	0.55	0.45	6	222	92	53	0.04	0.26	1.5×10^{-3}
3	0.84	1.04	10	158	62	(14)	0.18	0.51	1.4×10^{-2}

As an example, the filtered components from $\Delta_T = 3$ cm are shown in figure 1d. For time $t < T_i$, the amplitude of the H1 seiche increases to a maximum non-resonantly forced value, which we define as η_o. This allows the potential energy introduced by the forcing mechanism per cycle to be estimated $P \approx (1/6)gL(\rho_2 - \rho_1)\eta_o^2$ [4]. The tank was forced for six cycles and resonant amplification of the H1 seiche occurs over approximately $T_i < t < 7T_i$. During this period the energy content of the surge and NLIWs is also increased. Interestingly, a steady-state baroclinic tilt of the interface is evident as a vertical translation of the H1 seiche signal, relative to an equilibrium level of zero, during resonant forcing. The baroclinic tilt results from the forcing mechanism being consistently in the same direction (i.e. to reproduce periodic wind events from the same direction along the main axis, the end of the tank was only rotated above the horizontal position as opposed to both above and below horizontal). The tilt is not evident in the surge and NLIWs since these signals were band-pass filtered, whereas the seiche was low-pass filtered. Upon termination of the periodic forcing $t > 6T_i$, the baroclinic tilt is no longer observed and the seiche oscillates about the equilibrium position.

Under non-resonant conditions, the energy content of each component is proportional to the wavelength [4]. Similarly, resonant energy amplification of each component (expressed as a fraction of P) is also directly proportional to wavelength (table 1). However, perhaps surprisingly amplification is inversely proportional to η_o (over $0 < eta_o < h_1$). The baroclinic tilt has much less energy than the periodic wave motions ($< 10\%P$).

4.3. *Mixing and dissipation*

The Kelvin-Helmholtz instabilities observed to form within the progressive nonlinear internal waves are shown in figure 3 to cause diapycnal mixing. This mixing can be quantified following the procedure in [9]. The increase in potential energy per cycle b is obtained by dividing the increase in potential energy during the experiment (from figure 4) by the number of cycles during which strong mixing was observed to occur (6 cycles). When resonantly forced, the wave field is in steady-state (figure 1d), the energy input per cycle must equal the energy flux to mixing and dissipation $P = b + \epsilon$ and the mixing efficiency $R_f = b/P$ may be calculated (table 1). In agreement with previous studies, R_f is less than $\sim 20\%$ and scales with the intensity of the turbulence [11, 8, 9, 12]. Similarly, assuming an interface (metalimnion) thickness of $\delta_\rho \approx$ 2.5 cm (figure 4) with a bulk buoyancy frequency $N^2 \sim (g/\rho_o)(\rho_2 - \rho_1)/\delta_\rho \sim 7.8$

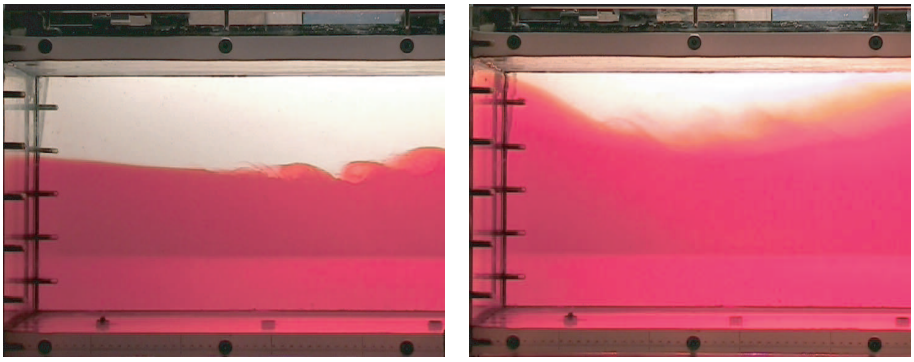

Figure 3. Video images of shear instabilities occurring within the high-frequency NLIWs of depression under resonant conditions. The NLIWs are propagating from right to left. Partial reflection from the left end wall is occurring. The field of view is 0.5 m by 0.5 m, the upper clear layer is fresh water (this layer appears white due to the backdrop) and the lower red layer is saline water. The left image was taken early in an experiment when the interface is thin, while the right image was acquired after the interface had thickened appreciably due to mixing.

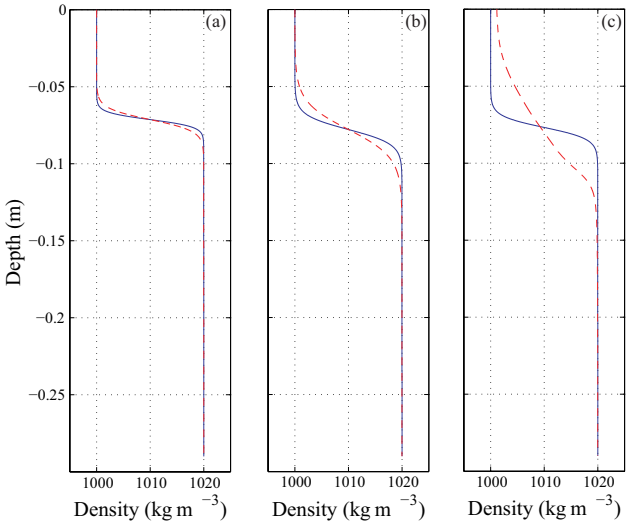

Figure 4. Measurements of the vertical density structure with the fluid quiescent both before and after the forcing events. (a) Run $\Delta_T = 1$ cm, (b) run $\Delta_T = 2$ cm and (b) run $\Delta_T = 3$ cm.

rad^2 s^{-2}, the average metalimnetic rate of dissipation $\epsilon \sim P - b$ and diascalar flux $K_\rho \sim (R_f/(1 - R_f))(\epsilon/N^2)$ may also be estimated over each wave period/forcing cycle [8] (table 1). The range 10^{-2} m^{2}s$^{-1} < K_\rho < 10^{-4}$ m^{2}s^{-1} is reasonable for energetic resonantly forced systems in comparison to observed values [2, 15] and as with R_f, K_ρ also scales with the intensity of the turbulence. These calculations should be considered approximate; the theory was developed for systems with constant N but we have applied a bulk N, estimated from the hyperbolic tangent density profiles (figure 4).

5. Discussion and generalization

Resonance was observed in a periodically forced basin over $(2/3)f_{H1} < f < 2f_{H1}$. Under resonant conditions, the internal wave field was decomposed into a steady baroclinic tilt, a H1 seiche, a nonlinear surge and high-frequency NLIWs. A downscale energy cascade was observed between the wave components, which occur at discrete frequencies [4]. The results suggest that the basin-scale wave components have a limiting amplitude/energy content, which is dependent upon the strength of the forcing. Under resonant amplification, excess energy is ultimately lost irreversibly to dissipation and mixing at turbulent scales through Kelvin-Helmholtz

instabilities that form within progressive NLIWs. Our observations roughly support a theoretical model [5] for the limiting critical amplitude a_c of NLIWs due to shear-induced decay; $a_c = 2\sqrt{\delta_\rho h_1} = 9$ cm , which may be compared to ≈ 7 cm from figure 1d. Note that the NLIW amplitude [2] and a_c are independent of η_o.

Progressive NLIWs (e.g. solitary waves) formed upon the resonating H1 seiche when $W^{-1} >\sim 0.03$. For $W^{-1} >\sim 0.5$, Kelvin-Helmholtz instabilities were observed to form within the progressive nonlinear internal waves, leading to diapycnal mixing within the basin interior. The impact of resonant amplification on inducing mixing is evident in comparison to run-down experiments [6], where $W^{-1} \sim 1$ was required for shear instability in the interior. The results may be generalized to real lakes and reservoirs using $W^{-1} \sim \eta_o/h_1 \sim Lu_*^2/g'h_1^2$, where u_* is related to the applied wind stress by $\tau = \rho u_*^2$ [6].

It is unlikely that the mid-basin ϵ and $K\rho$ estimates will be realized in all natural lakes and reservoirs. While shear-induced mixing has been observed in the interior of lakes (e.g. [2]), vertical mixing occurs predominantly within the benthic boundary layer [7, 14]. The presence of sloping topography in natural systems will cause the NLIWs to break on shoaling topography at the lake perimeter, locally energizing the benthic boundary layer at the depth of the thermocline [3].

Acknowledgments

Funding was from the Australian Research Council and Queen's University.

References

[1] J. P. Antenucci and J. Imberger. The seasonal evolution of wind/internal wave resonance in Lake Kinneret. *Limnol. Oceanogr.*, 48:2055–2061, 2003.

[2] L. Boegman, J. Imberger, G. N. Ivey, and J. P. Antenucci. High-frequency internal waves in large stratified lakes. *Limnol. Oceanogr.*, 48:895–919, 2003.

[3] L. Boegman, G. N. Ivey, and J. Imberger. The degeneration of internal waves in lakes with sloping topography. *Limnol. Oceanogr.*, 50:1620–1637, 2005.

[4] L. Boegman, G. N. Ivey, and J. Imberger. The energetics of large-scale internal wave degeneration in lakes. *J. Fluid Mech.*, 531:159–180, 2005.

[5] D. Bogucki and C. Garrett. A simple model for the shear-induced decay of an internal solitary wave. *J. Phys. Oceanogr.*, 23:1767–1776, 1993.

[6] D. A. Horn, J. Imberger, and G. N. Ivey. The degeneration of large-scale interfacial gravity waves in lakes. *J. Fluid Mech.*, 434:181–207, 2001.

[7] J. Imberger. Flux paths in a stratified lake: a review, p. 1–18. In *J. Imberger [ed.], Physical processes in lakes and oceans.*, volume 54 of *Coastal and Estaurine Studies*. 1998.

[8] G. N. Ivey and J. Imberger. On the nature of turbulence in a stratified fluid. Part 1: The energetics of mixing. *J. Phys. Oceanogr.*, 21:650–658, 1991.

[9] H. Michallet and G. N. Ivey. Experiments on mixing due to internal solitary waves breaking on uniform slopes. *J. Geophys. Res.*, 104:13467–13477, 1999.

[10] M. Münnich, A. Wüest, and D. M. Imboden. Observations of the second vertical mode of the internal seiche in an alpine lake. *Limnol. Oceanogr.*, 37:1705–1719, 1992.

[11] T. R. Osborn. Estimates of the local rate of vertical diffusion from dissipation measurements. *J. Phys. Oceanogr.*, 10:89–89, 1980.

[12] L. Shih, J. R. Koseff, G. N. Ivey, and J. H. Ferziger. Parameterization of turbulent fluxes and scales using homogeneous sheared stably stratified turbulence simulations. *J. Fluid Mech.*, 525:193–214, 2005.

[13] S. A. Thorpe. Near-resonant forcing in a shallow two-layer fluid: a model for the internal surge in Loch Ness? *J. Fluid Mech.*, 63:509–527, 1974.

[14] A. Wüest, G. Piepke, and D. C.van Senden. Turbulent kinetic energy balance as a tool for estimating vertical diffusivity in wind-forced stratified waters. *Limnol. Oceanogr.*, 45:1388–1400, 2000.

[15] P. S. Yeates and J. Imberger. Turbulent kinetic energy balance as a tool for estimating vertical diffusivity in wind-forced stratified waters. *Intl. J. River Basin Management*, 1:297–319, 2003.